



Fermi National Accelerator Laboratory

DTP/94/88
SACLAY/SPHT-T94/115
FERMILAB-CONF-94/350-T

Jet Physics at $P\bar{P}$ -colliders

W. T. Giele,¹

*Fermi National Accelerator Laboratory, P.O. Box 500,
Batavia, IL 60510, U.S.A.*

E. W. N. Glover

Physics Department, University of Durham, Durham DH1 3LE, UK

and

David A. Kosower

*Service de Physique Théorique, Centre d'Etudes de Saclay,
F-91191 Gif-sur-Yvette cedex, France*

We review recent theoretical developments in the calculation of jet cross sections in $P\bar{P}$ collisions. We present as examples comparisons between experimental results and next-to-leading order predictions for the inclusive di-jet sample. Such comparisons can provide constraints on the gluon density function for moderate parton momentum fractions.

1. Introduction

Understanding events with multiple jets in hadron colliders is essential to the extraction of new physics. Although jet cross sections are interesting in themselves as a test of QCD, the main reason for studying them is to understand and predict such final states to a high level of accuracy. Only then can one extract any new physics manifested in deviations from the expected QCD background.

¹presented at the Workshop on "Radiative Corrections: Status and Outlook" June 27 - July 1 1994, Gatlinburg TN.



A good, and topical, example is the measurement of top quark kinematics at Fermilab. In order to study this physics, it is important to measure accurately the top quark decay modes $P\bar{P} \rightarrow l^\pm \nu + \geq 4 \text{ jets}^1$ and $P\bar{P} \rightarrow \geq 6 \text{ jets}^2$. These decay modes allow the (partial) reconstruction of the top quark momenta. There are however substantial QCD backgrounds in these channels. To extract information on the kinematics of the top quark one must be able to predict the backgrounds with large jet multiplicities reliably. Numerous other new physics searches involve signals which contain multiple jets and hence a good understanding of the backgrounds becomes important.

As we shall describe in section 2, high-multiplicity jet cross sections are at present known only to leading order in α_s . The next-to-leading order cross sections are known for a few processes: $P\bar{P} \rightarrow V + \geq 0, 1 \text{ jets}^3$ (where $V = W^\pm, Z^0, \gamma$) and $P\bar{P} \rightarrow \geq 2 \text{ jets}^4, 5, 6$. An important question these calculations can address is the determination of those regions of phase space where the leading order calculations are reliable, or in other words when perturbative QCD is applicable. The usual method of varying the renormalization scale to estimate the higher order corrections only probes the uncertainty associated with the ultraviolet behavior of the cross section. It fails to probe the infrared logarithms. In fact, these latter logarithms are usually the reason for the breakdown of the perturbative expansion; and thus the only way to estimate the uncertainty at leading order is to calculate the next-to-leading order corrections explicitly. In regions of phase space where the corrections are small one can trust the leading order predictions and next-to-leading order calculations will merely improve the prediction for the total event rate of the given final state. In regions where there are substantial corrections due to infrared logarithms, neither leading-order nor next-to-leading order calculations are reliable, and resummation of the large logarithms is in order. In the gray area in between, where there are noticeable corrections one can, with the necessary care, make use of the next-to-leading order predictions (although an estimate of the theoretical uncertainty is difficult).

There are two possible approaches to tackling the problem. The preferred way is to actually calculate the higher-order corrections for larger-multiplicity jet final states. We review the progress in this area in section 3. A weaker alternative is the study of leading-order and next-to-leading order calculations, and of data, for those cross sections where the next-to-leading order calculation exists, followed by extrapolation of the findings to larger jet-multiplicity cross sections. In section 4, we present some results of studies of the two-jet inclusive cross section where leading order, next-to-leading order, and data are compared.

2. Perturbative QCD and Jet Physics

The applicability of perturbative QCD to an observable depends in general on two assumptions. Firstly we must neglect hadronization effects; second, the perturbative

expansion has to be valid. This usually means we should examine scattering processes with a large momentum transfer and observables which are relatively insensitive to soft physics. Jets fulfill these requirements by construction, provided certain conditions on cone size and minimum transverse energy are satisfied. A jet is by definition a cluster of individual hadrons which are averaged out by the jet algorithm to give a single object with a well-defined direction. The minimal jet transverse-energy cut ensures that there is a substantial momentum transfer in the scattering. The averaging over individual hadrons ensures that jet distributions are not sensitive to the behavior of soft QCD radiation. From this viewpoint the jets can be considered opaque, that is in order to apply perturbative QCD one cannot ask detailed questions about the physics inside the jet cone, e.g. B -tagging of the jets or jet shapes and radiation patterns. Before one can apply perturbative QCD to such observables one has to rethink or reorder the perturbative expansion.

At leading order, the application of perturbative QCD to (opaque) jet cross sections identifies each jet axis, and each jet's energy with the direction and energy of an individual outgoing parton. At next-to-leading order the identification between a parton and a jet becomes more fuzzy, as a jet may consist of two partons which are averaged by the jet algorithm. This implies that at next-to-leading order the predictions become more sensitive to details of the jet algorithm. For any sensible jet algorithm these effects should be small, there otherwise the validity of the perturbative approach is undermined. In addition, next-to-leading order calculations reduce substantially the renormalization and factorization scale dependences compared to leading order calculations, making a more reliable prediction of the event rates possible.

All in all, the perturbative approach gives a very systematic approach to calculating multiple jet cross sections. In practice, one expects that leading-order predictions will work well for hard, central, multiple-jet events. This are exactly the sorts of events one needs to predict reliably when searching for new physics consisting of heavy intermediate states, such as the top quark.

3. Theoretical Developments

Techniques for calculating leading order multiple parton amplitudes have been developed to a stage where one can construct all the phenomenologically relevant multi-jet cross sections at leading order. The key techniques for these calculations are the introduction of helicity amplitudes,⁷ color-ordered subamplitudes⁸ and recursion in the number of gluons.⁹ With these techniques leading-order multi-jet cross sections were calculated and embodied in weighted multijet event generators such as NJETS¹⁰ (for $P\bar{P} \rightarrow \geq n$ jets, where $n \leq 5$) and VECBOS¹¹ (for $P\bar{P} \rightarrow V + \geq n$ jets, where $n \leq 4$). If phenomenologically required, the number of final-state jets can be extended without significant difficulties.

These new insights into the calculus of tree graphs also allowed the calculation

of the singular behavior due to soft partons in processes with arbitrary number of partons. The key point here is the fact that color-ordered subamplitudes factorize in the soft limit.¹² That is, one obtains a soft factor times the hard subamplitude with the soft parton removed. In this respect the subamplitudes behave exactly like QED amplitudes, while the full QCD amplitude does not have such a simple factorization behavior (because of the color factors). With these observations it is possible to calculate analytically the soft contributions to next-to-leading order multiple-jet cross sections.¹³ The additional hard bremsstrahlung contributions can be added in numerically.

The only remaining part in a full next-to-leading order calculations is the computation of the virtual one-loop contributions. While the one-loop corrections for 2 parton \rightarrow 2 parton¹⁴ and 2 parton \rightarrow $V + 1$ parton¹⁵ were calculated a long time ago, no progress was made until recently. By employing again the concept of helicities and color ordered sub-amplitudes progress has been made in calculating the 2 \rightarrow 3 parton one-loop amplitudes. By using in addition string-based techniques, the five-gluon one-loop amplitude was calculated.¹⁶ The corrections to the four-quark plus one gluon loop amplitude have been calculated recently.¹⁷ The remaining one-loop two-quark three-gluon amplitude has also been completed recently.¹⁸ With these calculations all the ingredients required for the construction of a full next-to-leading order $P\bar{P} \rightarrow \geq 3$ jets event generator are available. Similar developments can be expected for the construction of the next-to-leading order $P\bar{P} \rightarrow V + \geq 2$ jets.

Furthermore, some more ambitious attempts are being made to calculate expressions for one-loop amplitudes with large numbers of partons. Possible approaches are developing recursion relations¹⁹ and/or using cutting rules.²⁰ These techniques might eventually lead to the possibility of going well beyond the next-to-leading order three-jet and vector boson plus two-jet calculations.

4. Di-jet production

Inclusive di-jet production (two jets + X) is of interest because it can provide direct constraints on the gluon distribution function. Both the CDF^{21,22} and D0 collaboration²³ have large samples of di-jet events. In addition, next-to-leading order calculations are available for the experimentally-measured distributions, which makes this particular final state interesting. Both theory and experiment can study the di-jet cross section in detail. The first goal of such a study is to establish whether the theoretical calculations suffice for reliable predictions of the observables, and secondly to constrain the parton density functions, especially the gluon density function. Here we will concentrate on the first step, namely asking under what circumstances is perturbative QCD valid for the triply-differential inclusive di-jet production.

For the theoretical predictions, we have used a weighted parton-level event generator, JETRAD.^{5,6,13} This allows us to build in the jet algorithm, detector acceptance

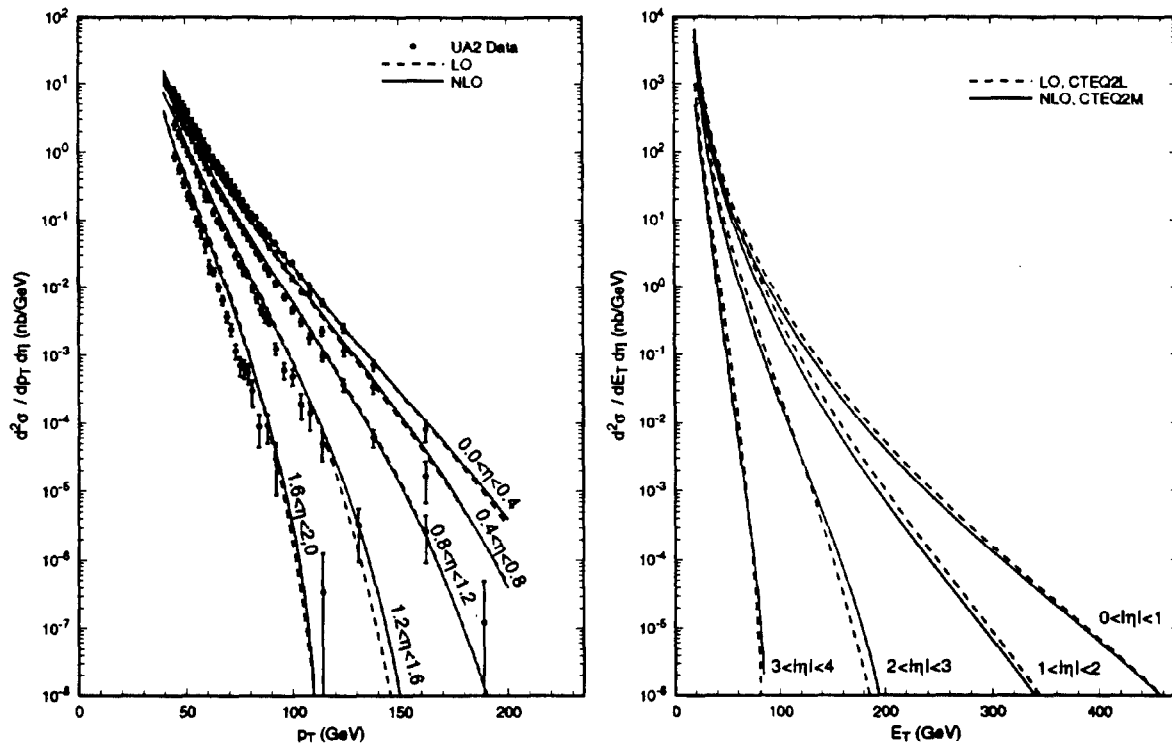


Figure 1: The one-jet differential transverse-energy distribution in different rapidity intervals. Both the leading-order (using the CTEQ2L parton density function) and next-to-leading order (using CTEQ2M) predictions are given for both the UA2 measurement²⁴ (left) and the D0 setup²³ (right).

and other analysis cuts numerically, thus duplicating the experimental setup within the theoretical prediction. It also makes it easy to construct the often-complicated observables within the numerical simulation. In all results shown, we take (unless otherwise stated) the renormalization/factorization scale to be the maximum transverse energy of the observed jets.

Before looking at the two-jet inclusive cross section, we will study the rapidity behavior of the jet in the one-jet inclusive sample. The one-jet inclusive transverse energy distribution has been studied and compared to theory extensively. To study the rapidity dependence we break up the transverse energy distribution in different rapidity regions to see whether the theory suffices when the jet is forward. The UA2 collaboration²⁴ published results for this particular distribution, while the D0 collaboration has so far shown only preliminary results²³. In figure 1 the predictions for the UA2 data and D0 setup are shown. As can be seen the next-to-leading order corrections are of a reasonable size (20%-30%), except for the most forward rapidity bin in the D0 experiment where the corrections increase to about 70%. This means the data should agree readily with the theory, except in the very forward regions.

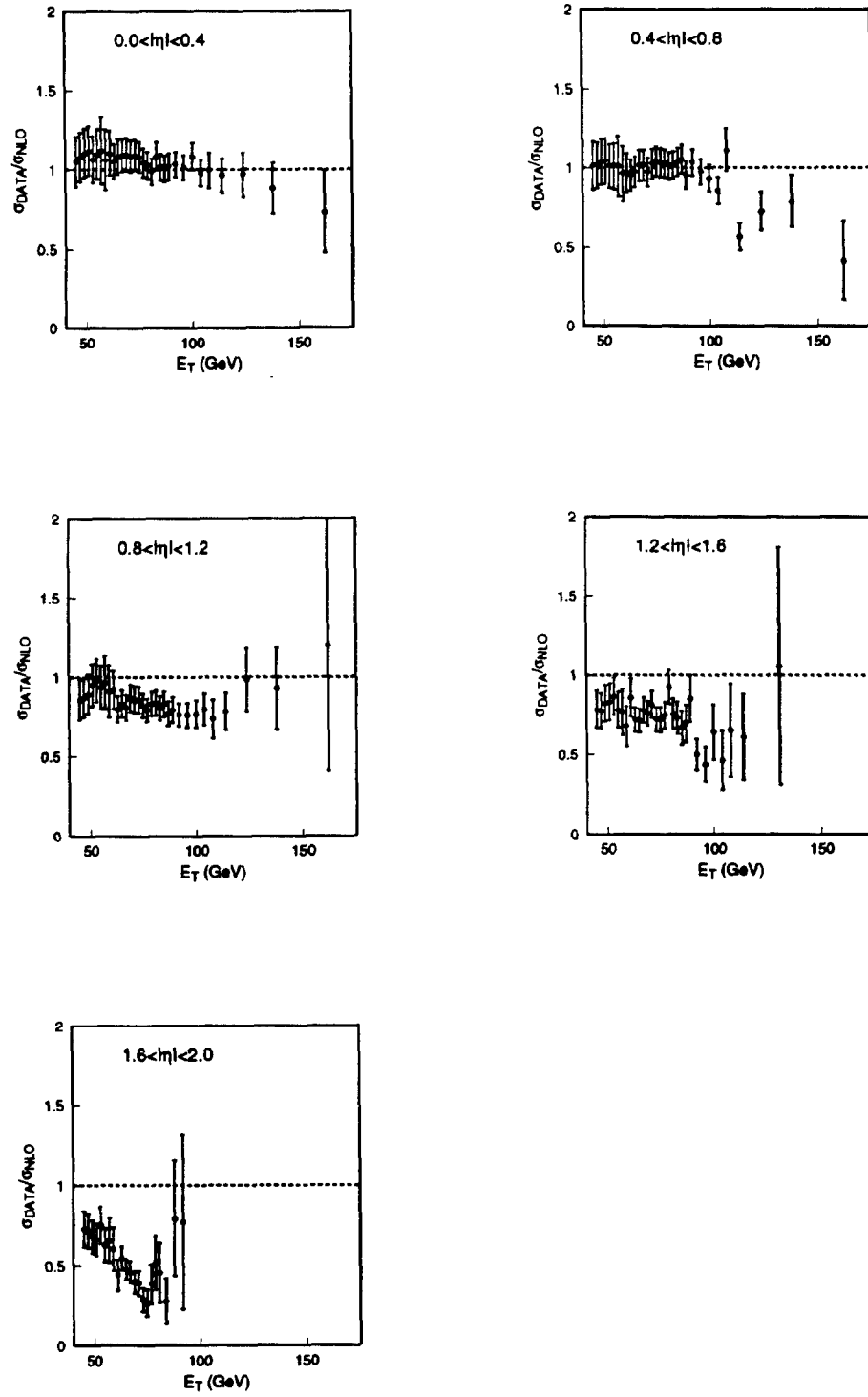


Figure 2: The ratio of the UA2 data²⁴ and the next-to-leading order predictions as presented in figure 1

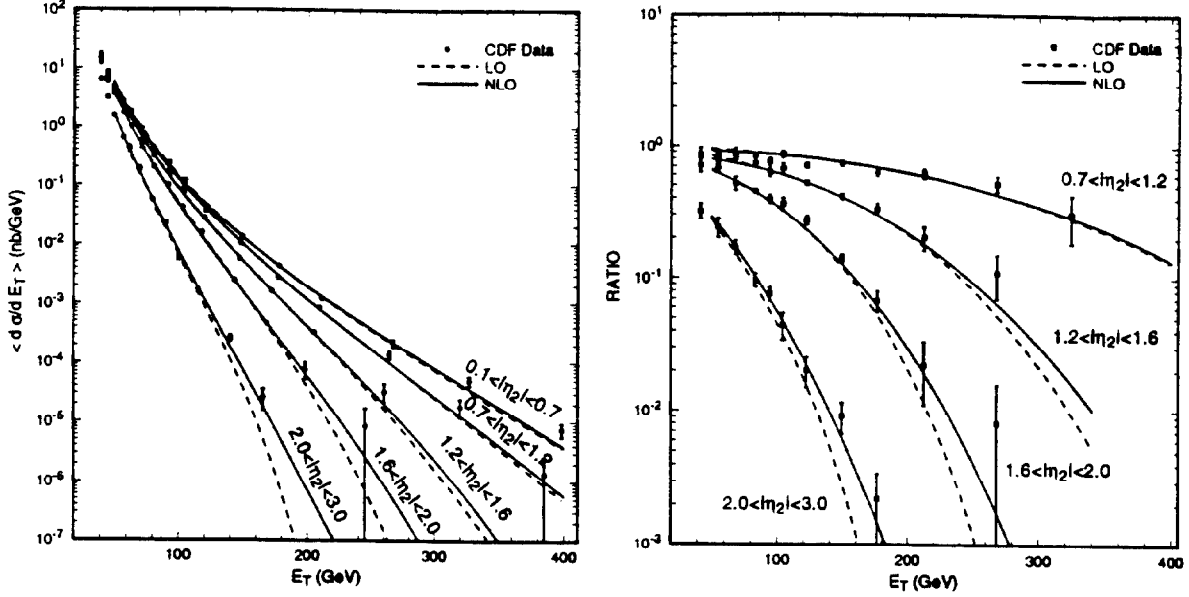


Figure 3: The transverse energy distribution of the central jet binned according to the rapidity of the second jet in inclusive di-jet production (left) and the ratio of the forward rapidity bin results over the central rapidity bin (right) at leading order (LO), at next-to-leading order⁵ (NLO), and with CDF data.²¹

To compare with the data we take the ratio of the UA2 data and the corresponding next-to-leading order prediction, the result is shown in figure 2. The comparison is very reasonable as expected, though for the larger rapidity bins the data seems to be slightly lower than the theory. It will be interesting to see how the more recent D0 data will compare with the theory, especially in the more forward rapidity regions not covered by the UA2 measurement. If the same trend appears one has to understand the reason for this discrepancy and whether its basis lies in the input parton density functions.

The next step is to look at the triply-differential cross section, $\frac{d^3\sigma}{dE_t d\eta_1 d\eta_2}$. Both CDF^{21,22} and D0²³ have started exploring this cross section. The first two published results are from the CDF collaboration and consider a one-dimensional projection of the triply-differential cross section. This is a first step in exploring this cross section which ultimately should lead to direct constraints on the gluon parton density function for the parton momentum fractions in the range $10^{-2} - 10^{-1}$. There are no experimental results available which constrain the gluon density in this range, making

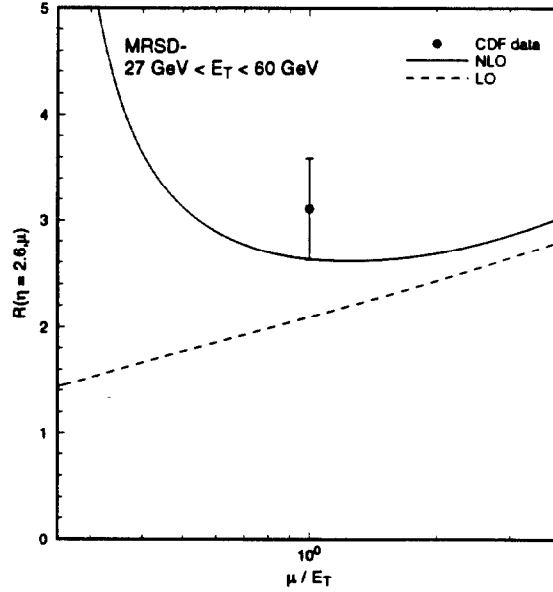


Figure 4: The scale variation of the ratio of same-side and opposite-side cross sections at $\eta = 2.6$ at leading order (LO) and next-to-leading order (NLO)⁶ for $27 \text{ GeV} < E_T < 60 \text{ GeV}$, $\mu = E_T$ and the MRSD- structure functions. Also shown is the CDF data point.²²

this a valuable measurement. Using the published CDF results we can have a first look at the theoretical predictions and uncertainties in these observables.

The first CDF publication²¹ examines the transverse energy behavior when one of the jets is required to be in the central rapidity bin ($0.1 \leq \eta_1 \leq 0.7$) while the second jet is required to be in one of the five rapidity bins. A distribution is made of the transverse energy of the central jet for all five bins. The results together with the next-to-leading order theoretical predictions⁵ are given in figure 3. Also shown is the ratio of the distributions with the central distribution (where both jets are required to have a rapidity between 0.1 and 0.7). The renormalization scale variation affects only the overall normalization of the distribution in a relevant way. The shape of the distribution at next-to-leading is very stable under the scale variation. The largest next-to-leading order normalization uncertainty is in the most forward rapidity bin and is of the order of 10%. As can be seen for the central rapidity regions leading order, next-to-leading order and data readily agree. However in the forward regions, especially at larger transverse energies, the leading-order prediction is substantially smaller than next-to-leading order. The reason for this is simply a kinematical effect in $2 \rightarrow 2$ scattering: requiring the parton momentum fractions to be smaller than 1 and fixing the rapidities of both jets (at leading order both partons) restricts the transverse energy of the jets. For example, in the $2.0 < \eta_2 < 3.0$ bin the maximum transverse energy for the jet at leading order is around 210 GeV, whereas at next-to-leading order this limit is increased significantly because $2 \rightarrow 3$ particle scattering is

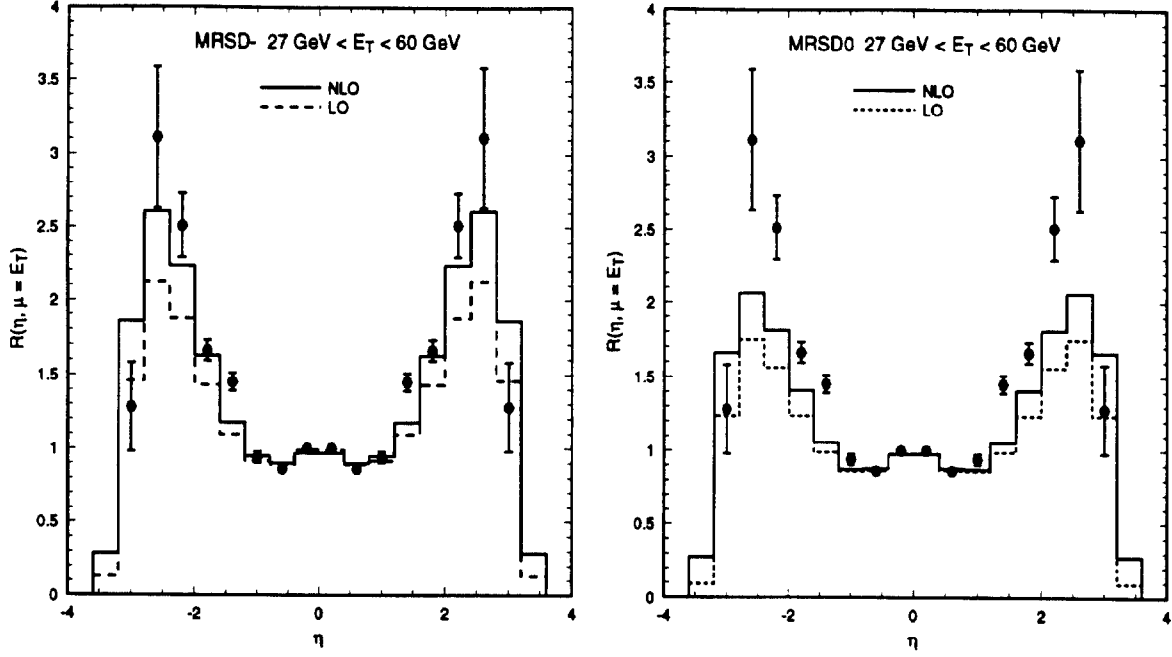


Figure 5: The ratio of same-side and opposite-side cross sections at next-to-leading order⁶ (NLO) and leading order (LO) as a function of η for $27 \text{ GeV} < E_T < 60 \text{ GeV}$, $\mu = E_T$ and (a) MRSD- (b) MRSD0 structure functions. Also shown is the preliminary CDF data²²

included. As can be seen from figure 3 the data extends close to this kinematical limit and the next-to-leading order calculation is needed to describe the measurement.

In order to constrain the parton density functions, it is more useful to look at the rapidity distributions of the di-jet system at a fixed transverse energy (or transverse energy slice) of the leading jet, $\frac{d^2\sigma}{d\eta_1 d\eta_2}$. By comparing this two-dimensional distribution with the data one can extract information about the parton density functions and, provided the transverse energy is not too large, obtain direct constraints on the gluon densities in ranges of parton fractions not accessible to other experiments. Studying the full two-dimensional distribution is complicated in both experiment and theory. However one can first gain some confidence by looking at one dimensional distributions derived from the double differential rapidity distribution. The D0 collaboration is looking at the distribution of the variable $\eta_1 \times \text{sign}(\eta_2)$, no data is published yet.²³ On the other hand, the CDF collaboration has published results on the so-called same-side over opposite-side two-jet ratio.²² Here one looks at the ratio of two cross sections. The same side cross section is simply the cross section as a function of the rapidity where both jets have the same rapidity, while in the opposite

side cross section the jets are required to have opposite rapidities:

$$\begin{aligned}\sigma_{\text{same side}}(\eta) &= \left. \frac{d^2\sigma}{d\eta_1 d\eta_2} \right|_{\eta_1=\eta_2=\eta} \\ \sigma_{\text{opposite side}}(\eta) &= \left. \frac{d^2\sigma}{d\eta_1 d\eta_2} \right|_{\eta_1=-\eta_2=\eta}.\end{aligned}$$

An added advantage of the ratio is that a many experimental and theoretical uncertainties cancel. The leading order prediction for the ratio does not depend on the renormalization scale. The only scale dependence comes through the factorization scale present in the parton densities. At next-to-leading order this changes due to the presence of the strong coupling constant. Both the leading and next-to-leading order renormalization scale dependence at a fixed rapidity of 2.6 are shown in figure 4.⁶ Note that the leading order behavior under scale variation is just a logarithmic scaling, while the next-to-leading order behavior is more complicated. The scale choice used is the transverse energy of the leading jet which corresponds to the minimum of the curve. With this scale choice we have calculated at leading and next-to-leading order the same-side to opposite-side ratio with two different parton density function sets, MRSD- and MRSD0. These two sets represent the extremes in the small- x behavior². The results are shown in figure 5.⁶ Note that using next-to-leading order in combination with the more singular MRSD- structure function is consistent with the CDF data, while the MRSD0 set is clearly disfavored by the data.

The following step would be the study of the shape of the two-dimensional rapidity distribution.²⁵ This distribution has a larger sensitivity to the parton density functions than the same side over opposite side ratio. The ratio already discriminates well between different parton density sets, making the prospects for using the full di-jet rapidity correlations to constrain the parton densities very promising.

Conclusions

Jet physics at $P\bar{P}$ colliders is evolving quickly both experimentally and theoretically. With the current and forthcoming data sets, both the CDF and D0 collaborations will be able to study multi-jet final states in great detail. The di-jet inclusive sample can be used to constrain the parton density functions, and in particular, will provide direct constraints on the gluon density function in the parton fraction range between $10^{-2} - 10^{-1}$. The next-to leading order calculations should have sufficient accuracy for this purpose.

More theoretically, the next-to-leading order soft contributions to multi-jet production are well understood. However the calculations of the one-loop contributions are still cumbersome, although some progress has been made in understanding these complicated calculations. Within the foreseeable future next-to-leading order event

²For $xg(x)$ MRSD- behaves as $x^{-0.5}$ while MRSD0 behaves as x^0 at small x

generators can be expected for inclusive three-jet and vector boson + two-jet production at $P\bar{P}$ colliders. This will open a new area of phenomenological study using multi-jet production.

References

1. W.T. Giele and W.J. Stirling, *Nucl. Phys.* **B343** (1990) 14;
H. Baer, V. Barger and R.J.N. Phillips, *Phys. Rev.* **D42** (1990) 54;
F.A. Berends, J.B. Tausk and W.T. Giele, *Phys. Rev.* **D47** (1993) 2746;
V. Barger, J. Ohnemus and R.J.N. Phillips, *Phys. Rev.* **D48** (1993) 3953;
J.M. Benlloch, K. Sumorok and W.T. Giele, *Nucl. Phys.* **B425** (1994) 3;
V. Barger, E. Mirkes, J. Ohnemus and R.J.N. Phillips, *Madison preprint*, MAD-PH-807 (Dec. 1993); *Madison preprint*, MAD-PH-849 (Sep. 1994);
The CDF collaboration, *Pisa preprint*, INFN-PI-AE-94-03 (Apr. 1994);
The CDF collaboration, *Phys. Rev.* **D50** (1994) 2966;
The D0 Collaboration, *Fermilab preprint*, FERMILAB-PUB-94-277 (Aug. 1994).
2. W.T. Giele, D.A. Kosower and H. Kuijf, *Nucl. Phys. (Proc. Suppl.)* **B23** (1991) 22;
J.M. Benlloch, N. Wainer and W.T. Giele, *Phys. Rev.* **D48** (1993) 5226;
The CDF collaboration, *Fermilab preprint*, FERMILAB-CONF-94-152-E (Jun. 1994).
3. P.B. Arnold and M.H. Reno, *Nucl. Phys.* **B319** (1989) 37;
R.J. Gonsalves, J. Pawlowski and C.F. Wai, *Phys. Rev.* **D40** (1989) 2245;
H. Baer and M.H. Reno, *Phys. Rev.* **D47** (1993) 3906;
W.T. Giele, E.W.N. Glover and D.A. Kosower, *Nucl. Phys.* **B403** (1993) 633;
Phys. Lett. **B309** (1993) 205.
4. F. Aversa, M. Greco, P. Chiappetta and J.P. Guillet, *Z. Phys.* **C46** (1990) 253;
S.D. Ellis, Z. Kunszt and D.E. Soper, *Phys. Rev. Lett.* **64** (1990) 2121; *Phys. Rev. Lett.* **69** (1992) 1496.
5. W.T. Giele, E.W.N. Glover and D.A. Kosower, *Fermilab preprint*, FERMILAB-PUB-94-070-T (to appear in *Phys. Rev. Lett.*).
6. W.T. Giele, E.W.N. Glover and D.A. Kosower, *Fermilab preprint*, FERMILAB-PUB-94-211-T (to appear in *Phys. Lett.*).
7. D. Danckaert, P. de Causmaecker, R. Gastmans, W. Troost and T.T. Wu, *Phys. Lett.* **B114** (1982) 203;
R. Kleiss, *Nucl. Phys.* **B241** (1984) 235;
Z. Xu, D.H. Zhang and L. Chang, *Nucl. Phys.* **B291** (1989) 392;

- J.F. Gunion and Z. Kunszt, *Phys. Lett.* **B161** (1985) 333;
 F.A. Berends and W.T. Giele, *Nucl. Phys.* **B294** (1987) 700.
8. F.A. Berends and W.T. Giele, *Nucl. Phys.* **B294** (1987) 700;
 M. Mangano, S.J. Parke and Z. Xu, *Nucl. Phys.* **B298** (1988) 653; *Nucl. Phys.* **B299** (1988) 673;
 M. Mangano, *Nucl. Phys.* **B309** (1988) 461.
 9. F.A. Berends and W.T. Giele, *Nucl. Phys.* **B306** (1988) 759;
 D.A. Kosower, *Nucl. Phys.* **B335** (1990) 23;
 H. Kuijf, *Doctoral Thesis*, Multi-Parton Production at Hadron colliders, RX-1335 LEIDEN (1991).
 10. F.A. Berends, W.T. Giele and H. Kuijf, *Phys. Lett.* **B232** (1989) 266; *Nucl. Phys.* **B333** (1990) 120;
 F.A. Berends and H. Kuijf, *Nucl. Phys.* **B353** (1991) 59.
 11. F.A. Berends, W.T. Giele and H. Kuijf, *Nucl. Phys.* **B321** (1989) 39;
 F.A. Berends, W.T. Giele, H. Kuijf, R. Kleiss and W.J. Stirling, *Phys. Lett.* **B224** (1989) 237;
 F.A. Berends, H. Kuijf, B. Tausk and W.T. Giele, *Nucl. Phys.* **B357** (1991) 32.
 12. F.A. Berends and W.T. Giele, *Nucl. Phys.* **B313** (1989) 595.
 13. W.T. Giele, E.W.N. Glover and D. A. Kosower, *Nucl. Phys.* **B403** (1993) 633.
 14. R.K. Ellis and J.C. Sexton, *Nucl. Phys.* **B269** (1986) 445.
 15. R.K. Ellis, D.A. Ross and A.E. Terrano, *Nucl. Phys.* **B178** (1981) 421.
 16. Z. Bern, L. Dixon and D.A. Kosower, *Phys. Rev. Lett.* **70** (1993) 2677.
 17. Z. Bern, L. Dixon and D.A. Kosower, *Slac Preprint*, SLAC-PUB-6663 (Sep. 1994).
 18. Z. Kunszt, A. Signer and Z. Trocsanyi, *Zurich ETH Preprint*, ETH-TH-94-14 (May 1994).
 19. G. Mahlon, *Phys. Rev.* **D49** (1994) 2197; *Phys. Rev.* **D49** (1994) 4438.
 20. Z. Bern, L. Dixon, D.C. Dunbar and D.A. Kosower, *Slac Preprint*, SLAC-PUB-6563 (Sep. 1994).
 21. The CDF collaboration, *Fermilab Preprint*, FERMILAB-CONF-93/210-E (1993)..
 22. The CDF collaboration, *Fermilab Preprint*, FERMILAB-CONF-93/203-E (1993).
 23. The D0 collaboration, *Fermilab Preprint*, FERMILAB-CONF-94-035-E (1994).

24. The UA2 collaboration, *Phys. Lett.* **B257** (1991) 232:
25. W.T. Giele, E.W.N. Glover and D.A. Kosower, in preparation.